Neurobiology of Aging xxx (2014) 1–11

Contents lists available at ScienceDirect

Neurobiology of Aging

journal homepage: www.elsevier.com/locate/neuaging

Brain connectivity and novel network measures for Alzheimer's disease classification

Gautam Prasad [a,b], Shantanu H. Joshi [b], Talia M. Nir [a,b], Arthur W. Toga [a,b], Paul M. Thompson [a,b,c,*], for the Alzheimer's Disease Neuroimaging Initiative (ADNI)[1]

[a] Imaging Genetics Center, Institute for Neuroimaging and Informatics, Keck School of Medicine of University of Southern California, Los Angeles, CA, USA
[b] Laboratory of Neuro Imaging, Institute for Neuroimaging and Informatics, Keck School of Medicine of University of Southern California, Los Angeles, CA, USA
[c] Department of Neurology, University of California, Los Angeles, School of Medicine, Los Angeles, CA, USA

ARTICLE INFO

Article history:
Received 2 May 2013
Received in revised form 18 April 2014
Accepted 18 April 2014

Keywords:
SVM
Classification
Sensitivity
Specificity
Maximum flow
Connectivity matrix
Alzheimer's disease
Network measures
Graph
Ranking

ABSTRACT

We compare a variety of different anatomic connectivity measures, including several novel ones, that may help in distinguishing Alzheimer's disease (AD) patients from controls. We studied diffusion-weighted magnetic resonance imaging from 200 subjects scanned as part of the Alzheimer's Disease Neuroimaging Initiative. We first evaluated measures derived from connectivity matrices based on whole-brain tractography; next, we studied additional network measures based on a novel flow-based measure of brain connectivity, computed on a dense 3-dimensional lattice. Based on these 2 kinds of connectivity matrices, we computed a variety of network measures. We evaluated the measures' ability to discriminate disease with a repeated, stratified 10-fold cross-validated classifier, using support vector machines, a supervised learning algorithm. We tested the relative importance of different combinations of features based on the accuracy, sensitivity, specificity, and feature ranking of the classification of 200 people into normal healthy controls and people with early or late mild cognitive impairment or AD.

1. Introduction

Current approaches used to classify Alzheimer's disease (AD) (Klöppel et al., 2008; Kohannim et al., 2010) rely on features such as volumetric measures from anatomic regions in magnetic resonance imaging (MRI) of the brain, cerebrospinal fluid biomarkers, apolipoprotein E genotype, age, sex, body mass index, and, in some cases, clinical and cognitive tests. Here, we attempted to improve our understanding of the best features for AD classification by studying the utility of a variety of brain connectivity measures derived from diffusion-weighted images (DWIs) of the brain. Some of the features we chose came from standard tractography-based maps of fiber connectivity (Rubinov and Sporns, 2010) between brain regions; we supplemented these with more novel features derived from a flow-based connectivity method (Prasad et al., 2013b). We aimed to understand the information contained in the raw connectivity matrices versus network measures derived from them; we used all the resulting features to differentiate diagnostic categories related to AD (e.g., mild cognitive impairment [MCI]). To do this, we employed support vector machines (SVMs), a machine learning algorithm for classification, to learn from training data and then classify a separate test set.

Cui et al. (2012) used SVMs to classify amnestic MCI based on features indexing anatomic atrophy through segmentations of T1-weighted MRI and fraction anisotropy values from diffusion images using tract-based spatial statistics. They ranked the features using Fisher scores and selected the best-performing subset using cross-validation. They achieved an accuracy of 71.09%, sensitivity of 51.96%, and specificity of 78.40% for the classification of amnestic

Submitted to *Neurobiology of Aging* (NIBAD Special Issue).
* Corresponding author at: Imaging Genetics Center, Institute for Neuroimaging and Informatics, Keck School of Medicine of University of Southern California, 2001 N. Soto Ave., Los Angeles, CA 90032, USA. Tel.: +323 442 7246; fax: +323 442 7247.
E-mail address: pthomp@usc.edu (P.M. Thompson).
[1] Many investigators within the ADNI contributed to the design and implementation of ADNI and/or provided data, but most of them did not participate in the analysis or writing of this report. A complete list of ADNI investigators may be found at http://adni.loni.usc.edu/wp-content/uploads/how_to_apply/ADNI_Acknowledgement_List.pdf.

0197-4580/$ – see front matter © 2014 Elsevier Inc. All rights reserved.
http://dx.doi.org/10.1016/j.neurobiolaging.2014.04.037

MCI. Our method differs in that we use only measures of connectivity from diffusion images for our feature set, and the ranking is computed within a set of features we are interested in evaluating. Laplacian regularized least squares was used to classify AD in Zhang and Shen (2011) where they tried to incorporate structural MRI, PET imaging data, and cerebrospinal fluid biomarker features from MCI into an AD classifier, which achieved a performance of almost 95% accuracy. In our case, we explore classification of both MCI and AD and focus on the information contained in different types of connectivity features. Cortical thickness features from structural MRI were evaluated by Eskildsen et al. (2012) using classification although they focused on conversion from MCI to AD and achieved accuracies ranging from 70% to 76% depending on the time to conversion, in contrast we used classification as a means to understand the information captured in measures of connectivity. The emphasis in the present study is to explore and understand which diffusion-based network measures are predictive of AD in contrast to the goal of optimizing the accuracy of classification in previous studies.

Our results and experiments seek to characterize the information contained in different features used to represent connectivity in the brain. This is related to the problem of feature selection methods (Guyon and Elisseeff, 2003), which rank features in a meaningful way to understand the ones that are important and those that can be discarded because they are redundant or irrelevant. One approach to select the best features (Peng et al., 2005) is to use mutual information to find the most relevant features for a target class. Another popular approach is the least absolute shrinkage and selection operator (Tibshirani, 1996) that uses a linear model and its regression coefficients to choose the best subset of features. De Martino et al. (2008) chose the most informative voxels in functional MR images using a recursive feature elimination approach that repeatedly trains an SVM model to remove features contributing a small amount to the training model. In our technique, we use the accuracy from classification to evaluate different types of brain connectivity features and to understand which ones may have an advantage to classifying MCI or AD. In addition, we used the SVMs to rank the features within the different feature sets to get a better description of what features were driving the classifier.

Our connectivity measure computation, classification framework, and ranking were applied to publicly available structural and diffusion MRI from the Alzheimer's Disease Neuroimaging Initiative (ADNI) (Mueller et al., 2005). We studied neuroimaging data from 200 subjects: 50 normal healthy controls, 38 people with late MCI (LMCI), 74 with early MCI (EMCI), and 38 AD patients.

We extracted measures of connectivity between 68 automatically parcellated regions of interest on the cortex using both fiber and flow connectivity methods and organized the information into connectivity matrices. From these connectivity matrices, we computed a variety of widely used network measures. These features were then fed into a repeated, stratified 10-fold cross-validation design, using SVMs to classify controls versus AD, controls versus EMCI, controls versus LMCI, and EMCI versus LMCI. Our results show a significant difference in the accuracy of various combinations of features that were used to distinguish between the various diagnostic groups.

2. Methods

2.1. Data

Our data were from 200 subjects scanned as part of ADNI-2, a continuation of the ADNI project in which diffusion imaging (among other scans) was added to the standard MRI protocol. The dataset included diffusion MRI data from 50 cognitively normal controls (C), 74 EMCI and 38 LMCI subjects, and 38 people with AD.

Table 1
The demographic details for our age- and sex-matched sample

	All	NC	EMCI	LMCI	AD
N	200	50	74	38	38
Sex	115 M/85 F	23 M/27 F	46 M/28 F	24 M/14 F	22 M/16 F
Age	73.1 ± 7.5	72.4 ± 6.2	72.5 ± 8.0	72.6 ± 5.6	75.8 ± 9.1

The number of subjects (*N*), sex, and age are given for the full sample (all), elderly NCs, EMCI and LMCI subcategories, and AD patients. We carried out 2-sample *t* tests comparing age and sex between all pairs of subcategories and found no significant differences that passed the multiple comparison threshold.
Key: AD, Alzheimer's disease; EMCI, early mild cognitive impairment; F, female; LMCI, late MCI; M, male; NC, normal controls.

Subjects were scanned on 3-T GE Medical Systems scanners, which collected both T1-weighted 3-dimensional anatomic spoiled gradient-echo sequences (256×256 matrix, voxel size $= 1.2 \times 1.0 \times 1.0$ mm^3, inversion time $= 400$ ms, repetition time $= 6.98$ ms, echo time $= 2.85$ ms, and flip angle $= 11°$) and DWIs (256×256 matrix, voxel size $2.7 \times 2.7 \times 2.7$ mm^3, scan time $= 9$ minutes). Per subject, the DWIs consisted of 41 diffusion images with $b = 1000$ seconds/mm^2 and 5 T2-weighted b_0 images. This protocol was chosen after an effort to study trade-offs between spatial and angular resolutions in a tolerable scan time (Jahanshad et al., 2011).

The groups were matched in both age and sex that we confirmed using 2-sample *t* tests and multiple comparison correction. Detailed demographic information for each subgroup of subjects is listed in Table 1.

2.1.1. Image preprocessing

We processed the T1-WIs to parcellate them into 68 cortical regions. We first automatically removed extracerebral tissues from the anatomic images using ROBEX (Iglesias et al., 2011a), a method that learned from manual segmentations of hundreds of healthy young adults. Skull-stripped brains were inhomogeneity corrected using the N3 tool of the Montreal Neurologic Institute (Sled et al., 1998) and aligned to the Colin27 template (Holmes et al., 1998) with the Oxford Centre for Functional Magnetic Resonance Imaging of the Brain (FMRIB)'s Linear Image Registration Tool (FLIRT) (Jenkinson et al., 2002).

Table 2
List of the 34 regions that are segmented in the cortex by FreeSurfer in each hemisphere, making a total of 64 regions

Cortical regions			
1.	Banks of the superior temporal sulcus	18.	Pars orbitalis
2.	Caudal anterior cingulate	19.	Pars triangularis
3.	Caudal middle frontal	20.	Peri calcarine
4.	Cuneus	21.	Postcentral
5.	Entorhinal	22.	Posterior cingulate
6.	Fusiform	23.	Precentral
7.	Inferior parietal	24.	Precuneus
8.	Inferior temporal	25.	Rostral anterior cingulate
9.	Isthmus of the cingulate	26.	Rostral middle frontal
10.	Lateral occipital	27.	Superior frontal
11.	Lateral orbitofrontal	28.	Superior parietal
12.	Lingual	29.	Superior temporal
13.	Medial orbitofrontal	30.	Supramarginal
14.	Middle temporal	31.	Frontal pole
15.	Parahippocampal	32.	Temporal pole
16.	Paracentral	33.	Transverse temporal
17.	Pars opercularis	34.	Insula

These regions represent the nodes in the connectivity network for both the fiber and flow connectivity methods. In the network, each method calculated the connectivity strength between all pairs of regions. For fiber connectivity, this is computed as the number of tractography fibers that connect the 2 regions and for the flow connectivity it is computed using an approximate maximum-flow algorithm between the regions.

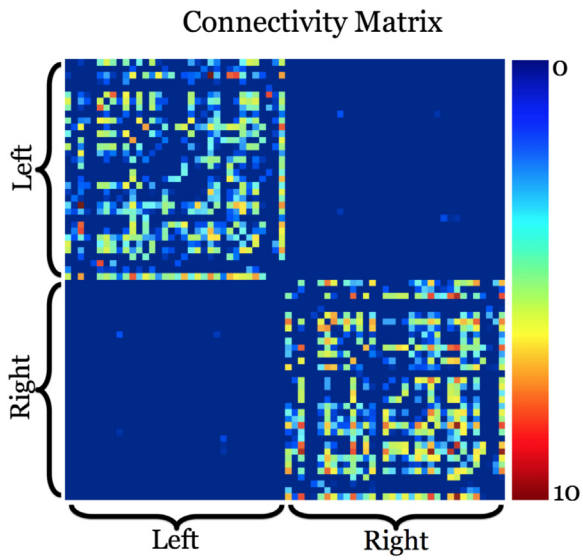

Fig. 1. We present an example 68 × 68 flow-connectivity matrix from our data. This matrix was derived using a flow-connectivity method that computed the maximum amount of flow between pairs of regions of interest on the cortex. In this subject, the connections within each hemisphere are far more extensive than those across the hemispheres. A brighter color means there is a stronger connectivity (in the sense of greater normalized fiber counts) between the 2 areas. We use this matrix, along with the standard fiber connectivity matrix, to compute network topology measures. These are then used in a machine-learning model to classify different disease states in our data.

The resulting images were segmented into 34 cortical regions (in each hemisphere) using FreeSurfer (Fischl et al., 2004) and are listed in Table 2. These segmentations were then dilated with an isotropic box kernel of 5 × 5 × 5 voxels to make sure they intersected with the white matter for subsequent connectivity analysis.

We corrected head motion and eddy current distortion in each subject by aligning the DWIs to the average b_0 image with FSL's eddy correct tool. The brain extraction tool (Smith, 2002) was then used to skull strip the brains. We corrected echoplanar imaging (EPI) distortion in these images with an elastic mutual information registration algorithm (Leow et al., 2007) that aligned the DWIs to the T1-weighted scans. Preprocessing steps are further detailed in Nir et al. (2012).

We used a global probabilistic tractography method based on the Hough transform (Aganj et al., 2011). Although ADNI scans are not high angular resolution, because of the need for a fast scan, this method takes advantage of all the diffusion information provided at each voxel, parametrized by the orientation distribution function (ODF). The Hough method generates curves in the fiber space and scores them based on fractional anisotropy and the ODF at each point along the curve. Fractional anisotropy was computed from the single-tensor model of diffusion (Basser and Pierpaoli, 1996). ODFs at each voxel were computed with a normalized dimensionless estimator derived from Q-ball imaging (Aganj et al., 2010). This model is more accurate and outperforms the previous Q-ball imaging definition (Tuch, 2004), offering better detection of multiple fiber orientations (Aganj et al., 2010; Fritzsche et al., 2010) and additional information for the scoring function.

To generate close to 50,000 fibers per subject, we used an accelerated form of this tractography method (Prasad et al., 2013c). Our optimizations included an ODF look-up table and a randomized search of the parameter space, to generate fibers in <1/60 of the original time.

2.2. Connectivity features

We used features derived from brain connectivity matrices that categorize connections between different regions of interest on the cortex. From these matrices, we computed a set of network measures that quantify different network characteristics. We chose different subsets of these features in our experiments. We used the classification accuracy as a metric to understand the utility of the connectivity information captured, in the context of diagnostic classification of AD.

2.2.1. Connectivity matrix

We computed connectivity matrices using 2 methods. The first quantifies pairwise connectivity strength as the relative proportion of fibers connecting the 2 brain regions. The second is a novel method that computes the maximum flow between regions by interpreting the diffusion image as a network of pipes or a flow graph (these terms are defined further subsequently).

Our first method takes fibers computed using the accelerated Hough tractography method and computes the number that intersect pairs of regions from the 68 cortical areas. We used these

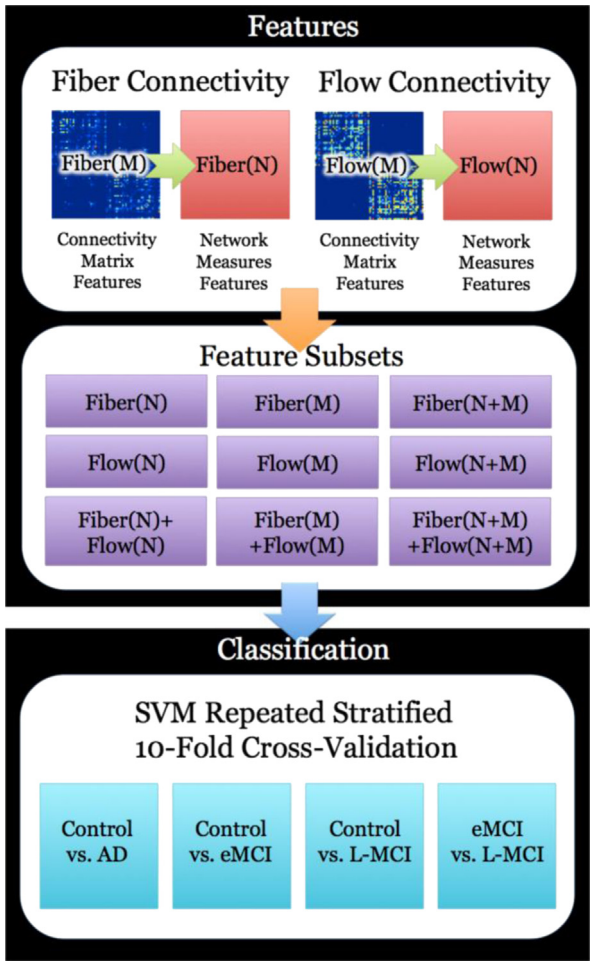

Fig. 2. A summary of how we select features of brain connectivity and classify them using support vector machines (SVMs). Our framework begins by computing hundreds of thousands of network measures from both fiber and flow connectivity matrices. We created 9 different subsets of features that are combinations of the network measures and raw connectivity matrices from a fiber and flow-based connectivity method. Each subset is evaluated by understanding their performance in classification problems based on the 4 different groups of subjects. These problems include control versus Alzheimer's disease (AD), control versus early mild cognitive impairment (EMCI), control versus late MCI (LMCI), and EMCI versus LMCI. For each problem, we used a stratified 10-fold cross-validated SVM classifier to understand how well the feature subset was able to discriminate between the 2 classes. The metrics used to evaluate the classifier performance were accuracy, sensitivity, and specificity.

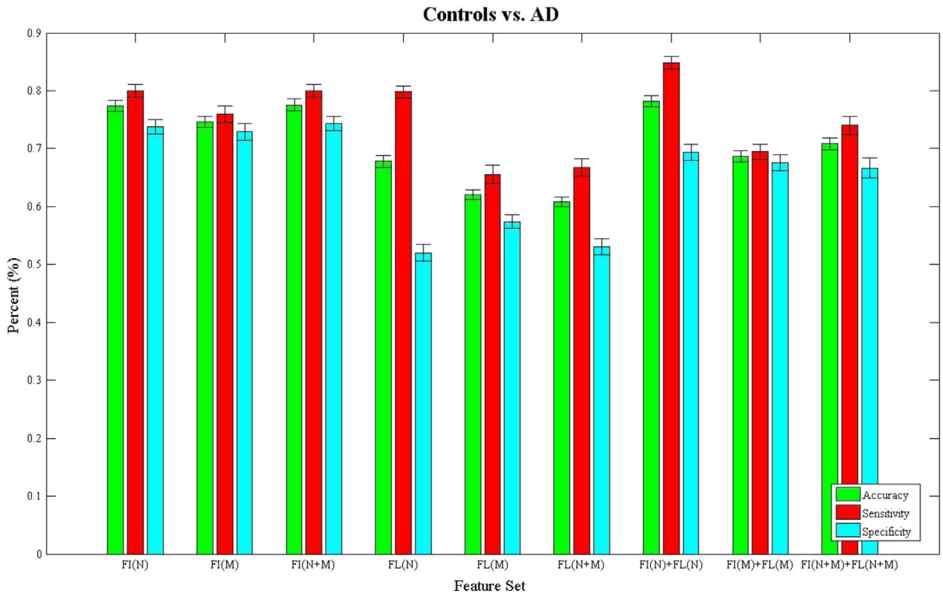

Fig. 3. We present the results from the stratified 10-fold cross-validated (CV) support vector machine classification of controls versus Alzheimer's disease (AD) using 9 subsets of connectivity features. These features come from both a fiber connectivity method (FI) and flow connectivity method (FL) and include a variety of graph-based network measures (N) along with the raw connectivity matrices (M). We evaluated the performance of each subset's ability to classify using accuracy, sensitivity, and specificity. The CV was repeated 30 times for each feature set using corresponding CV folds, and we evaluated differences using paired-sample *t* tests. The bar plot shows the mean accuracy, sensitivity, and specificity over the 30 CV results along with 95% confidence intervals. FI(N) + FL(N) had the highest accuracy of 78.2% and was not significantly different ($p > 0.05$) in performance from FI(N) and FI(N + M).

frequencies to populate a 68 × 68 connectivity matrix (with no normalization).

The second method we used is a flow-based measure of anatomic connectivity between all region pairs (Prasad et al., 2013a). In short, we first created a lattice network by connecting all lattice points (voxel centers) to all their immediate neighbors in 3 dimension. Edge weights were based on the ODF value in the direction of the edge. These edges were interpreted as pipes and their weight as the capacity of the pipe. In contrast with counting fibers between ROIs, we computed the maximum flow or capacity between each ROI pair, by following connecting tractography fibers projected onto the flow network

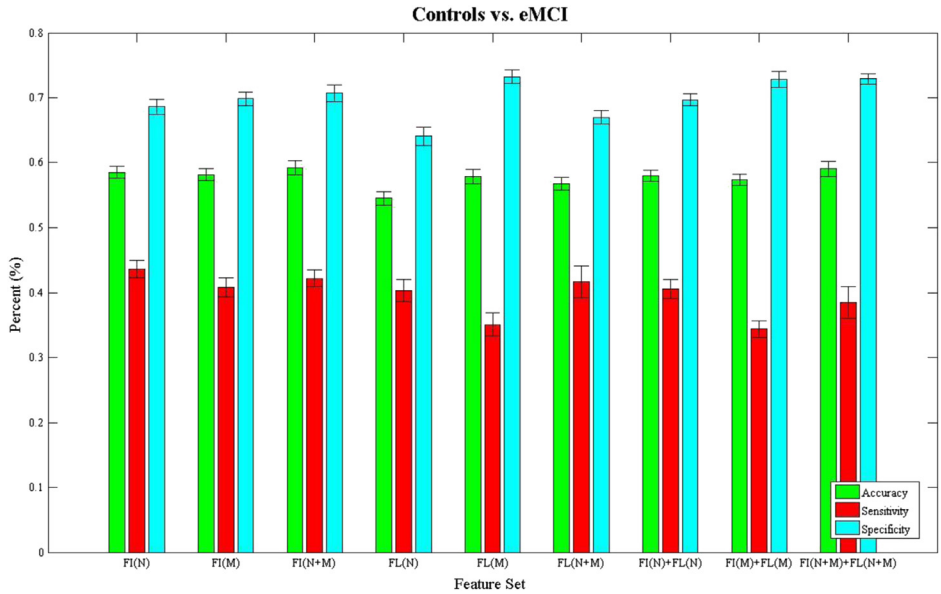

Fig. 4. We present the results from the stratified 10-fold cross-validated (CV) support vector machine classification of controls versus subject with early mild cognitive impairment (EMCI) using 9 subsets of connectivity features. These features come from both a fiber connectivity method (FI) and flow connectivity method (FL) and include a variety of graph-based network measures (N) along with the raw connectivity matrices (M). We evaluated the performance of each subset's ability to classify using accuracy, sensitivity, and specificity. The CV was repeated 30 times for each feature set using corresponding CV folds, and we evaluated differences using paired-sample *t* tests. The bar plot shows the mean accuracy, sensitivity, and specificity over the 30 CV results along with 95% confidence intervals. FI(N + M) had the highest accuracy of 59.2% and was not significantly different ($p >$ 0.05) in performance from FI(N + M) + FL (N + M).

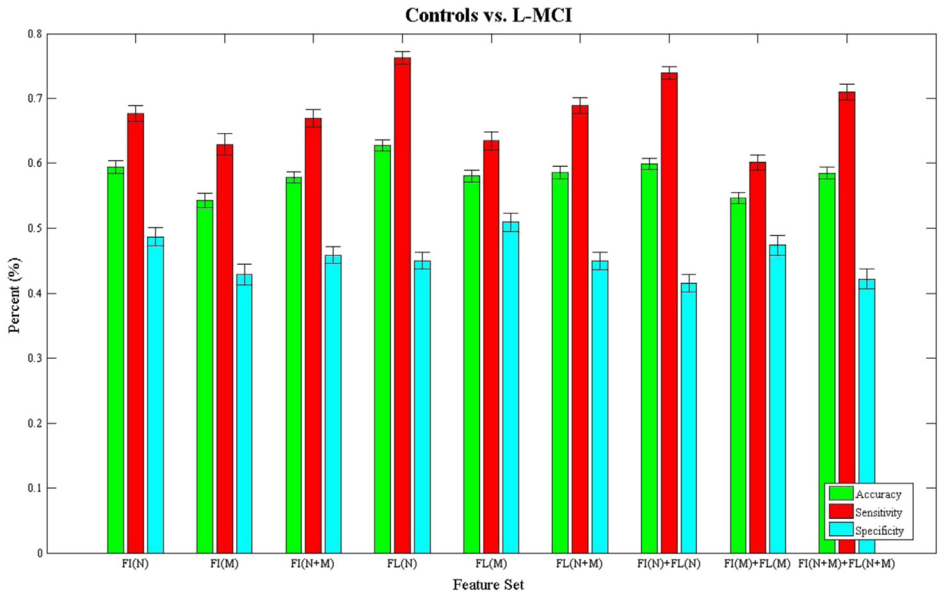

Fig. 5. We present the results from the stratified 10-fold cross-validated (CV) support vector machine classification of controls versus subject with late mild cognitive impairment (LMCI) subject using 9 subsets of connectivity features. These features come from both a fiber connectivity method (FI) and flow connectivity method (FL) and include a variety of graph-based network measures (N) along with the raw connectivity matrices (M). We evaluated the performance of each subset's ability to classify using accuracy, sensitivity, and specificity. The CV was repeated 30 times for each feature set using corresponding CV folds, and we evaluated differences using paired-sample *t* tests. The bar plot shows the mean accuracy, sensitivity, and specificity over the 30 CV results along with 95% confidence intervals. FL(N) had the highest accuracy of 62.8% and was significantly different ($p > 0.05$) in performance from all other subsets.

edges. We used a modified maximum-flow algorithm that is robust to noise in the diffusion data guided by biologically viable pathways and structure of the brain. The resulting flow is used to create a distinct 68 × 68 flow-connectivity matrix. Figure 1 gives an example flow-connectivity matrix using this method from our data. The lack of detected interhemispheric connections could be because most of them travel through the corpus callosum; so, it is difficult to detect fibers, for example, that connect frontal regions in the left hemisphere to the temporal regions in the right hemisphere. Additional research (Gong et al., 2009; Hagmann et al., 2008; Ingalhalikar et al., 2013) gives more examples of connectivity matrices that have similar interhemispheric and intrahemispheric distributions of connections.

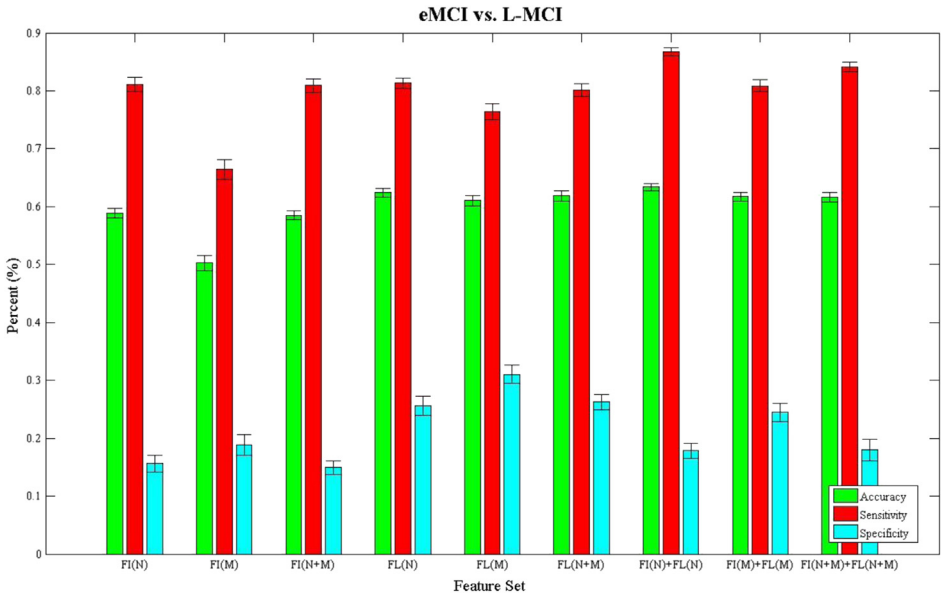

Fig. 6. We present the results from the stratified 10-fold cross-validated (CV) support vector machine classification of subjects with early mild cognitive impairment (EMCI) versus late MCI (LMCI) using 9 subsets of connectivity features. These features come from both a fiber connectivity method (FI) and flow connectivity method (FL) and include a variety of graph-based network measures (N) along with the raw connectivity matrices (M). We evaluated the performance of each subset's ability to classify using accuracy, sensitivity, and specificity. The CV was repeated 30 times for each feature set using corresponding CV folds, and we evaluated differences using paired-sample *t* tests. The bar plot shows the mean accuracy, sensitivity, and specificity over the 30 CV results along with 95% confidence intervals. FI(N) + FL(N) had the highest accuracy of 63.4% and was significantly different ($p >$ 0.05) in performance from all other subsets.

Table 3
The top 5 ranked features from each of the 9 feature subsets in the controls versus AD classification problem

Controls vs. AD										
Feature set	Rank 1/Th.		Rank 2/Th.		Rank 3/Th.		Rank 4/Th.		Rank 5/Th.	
FI(N)	Binary nodal Betweenness Centrality	0.5	Binary nodal Betweenness Centrality	0.6	Binary nodal Betweenness Centrality	0.7	Binary nodal Betweenness Centrality	0.8	Binary nodal Betweenness Centrality	0.9
FI(M)	R-entorhinal <->L-pars opercularis	0.2	R-fusiform <->L-pars opercularis	0.2	R-inferior parietal <->L-pars opercularis	0.2	R-inferior temporal <->L-pars opercularis	0.2	R-isthmus of the cingulate <->L-pars opercularis	0.2
FI(N + M)	Binary nodal Betweenness Centrality	0.5	Binary nodal Betweenness Centrality	0.6	Binary nodal Betweenness Centrality	0.7	Binary nodal Betweenness Centrality	0.8	Binary nodal Betweenness Centrality	0.9
FL(N)	Edge Neighborhood overlap	0.2	Edge Neighborhood overlap	0.2	Edge Neighborhood overlap	0.3	Matching index	0.2	Edge Neighborhood overlap	0.3
FL(M)	R-posterior cingulate <->L-parahippocampal	0.3	R-precentral <->L-parahippocampal	0.3	R-precuneus <->L-parahippocampal	0.3	R-rostral anterior cingulate <->L-parahippocampal	0.3	R-rostral middle frontal <->L-parahippocampal	0.3
FL(N + M)	Edge Neighborhood overlap	0.2	Edge Neighborhood overlap	0.2	Matching index	0.2	Edge Neighborhood overlap	0.3	Edge Neighborhood overlap	0.3
FI(N) + FL(N)	FL(N): strengths	0.1	FL(N): edge Neighborhood overlap	0.3	FL(N): edge Neighborhood overlap	0.3	FI(N): binary nodal Betweenness Centrality	0.5	FI(N): binary nodal Betweenness Centrality	0.6
FI(M) + FL(M)	FL(M): R-posterior cingulate <->L-parahippocampal	0.3	FL(M): R-precentral <->L-parahippocampal	0.3	FL(M): R-precuneus <->L-parahippocampal	0.3	FL(M): R-rostral anterior cingulate <->L-parahippocampal	0.3	FL(M): R-rostral middle frontal <->L-parahippocampal	0.3
FI(N + M) + FL(N + M)	FL(N): strengths	0.1	FL(N): edge Neighborhood overlap	0.3	FL(N): edge Neighborhood overlap	0.3	FI(N): binary nodal Betweenness Centrality	0.5	FI(N): binary nodal Betweenness Centrality	0.6

The features were computed using a fiber connectivity (FI) and flow connectivity (FL) methods using a variety of graph-based network measures (N) and the raw connectivity matrices (M). The network measures were computed from binary and weighted connectivity matrices that were filtered using a proportional threshold ranking from 0.1 to 1.0 (meaning all edges are retained) at intervals of 0.1. The features are shown along with their corresponding threshold (Th.). The ranking is derived from the support vector machine classification boundary and is averaged over each of the 10 cross-validated folds and 30 repeat runs. In cases that use features including the raw connectivity matrices at different thresholds, the label includes the 2 regions from the FreeSurfer segmentation that an edge connects. The symbol "<->" represents the undirected edge connecting the 2 regions in the connectivity network.
Key: AD, Alzheimer's disease; L, left; R, right.

2.2.2. Network measures

We represent the 2 types of connectivity matrices with network measures described in Rubinov and Sporns (2010) and computed them with the Brain Connectivity Toolbox. We derived these measures from both weighted and binary connectivity matrices: global efficiency, transitivity, path length, modularity, small world, radius, diameter, participation, local efficiency, optimal community structure, eigenvector centrality, and eccentricity. In addition, we computed density, number of vertices, number of edges, subgraph centrality, assortativity, nodal flow coefficient, average flow coefficient, total flow across central node, degree, matching index, edge neighborhood overlap, node pairs degree, and connected component sizes from only binary matrices and strengths from only weighted matrices. As is standard, 10 different thresholds were applied to each connectivity matrix, to preserve a fixed fraction of the weights ranging from 0.1 to 1, in intervals of 0.1.

In some cases, a network measure was computed for each node in the connectivity network, and this was the case for participation, local efficiency, and eigenvector centrality among others. This resulted in a vector of 68 values for a single network measure. For matching index or edge neighborhood overlap, the output was a 68×68 matrix of values. If a feature was multidimensional, we took the mean value in addition to its raw values. The results from each network measure were vectorized, and the entire set contained 14,930 features per threshold, making a total of 149,300 network measures per connectivity method. In addition, there are 2278 unique values from each connectivity matrix. These values represent the lower diagonal elements (not including the actual diagonal) and when factoring in the 10 thresholds make 22,780 connectivity matrix features per connectivity method. In total, there are (149,300 network measure features + 22,780 connectivity matrix features) × (2 connectivity methods: fiber and flow) = 344,160 possible features per subject.

2.3. Classification

SVMs (Cortes and Vapnik, 1995) are supervised learning models that we used to classify our connectivity features, to differentiate between disease states. SVMs classify 2-class data by training a model, or classification function, to find the best hyperplane between the 2 classes in the data. Let $x_i \in \mathbb{R}^d$ represent the connectivity feature vectors, where d is the dimension of the feature set of interest and $Y_i = \pm$ be their label with -1 and 1 representing 2 different disease states that could include controls, EMCI, LMCI, or AD. Our target hyperplane is as follows:

$$\langle w, x \rangle + b = 0,$$

where $w \in \mathbb{R}^d$ should separate as many data points as possible. We find it by solving the L2-norm problem:

$$\arg\min_{w,b,v} \left(\frac{1}{2} \langle w, w \rangle + D \sum_i v_i^2 \right),$$

such that

$$y_i(\langle w, x_i \rangle + b) \geq 1 - v_i,$$

$$v_i \geq 0,$$

where v_i are slack variables and D is a penalty parameter. In many instances, a hyperplane cannot be found to completely separate the

Table 4
The top 5 ranked features from each of the 9 feature subsets in the controls versus EMCI classification problem

Controls vs. EMCI										
Feature set	Rank 1/Th.		Rank 2/Th.		Rank 3/Th.		Rank 4/Th.		Rank 5/Th.	
FI(N)	Binary edge betweenness centrality	0.4	Binary edge betweenness centrality	0.5	Binary edge betweenness centrality	0.4	Binary edge betweenness centrality	0.6	Binary edge betweenness centrality	0.7
FI(M)	R-transverse temporal <->R-banks of the superior temporal sulcus	1.0	R-inferior parietal <->L-temporal pole	1.0	R-inferior temporal <->L-temporal pole	1.0	R-isthmus of the cingulate <->L-temporal pole	1.0	R-lateral occipital <->L-temporal pole	1.0
FI(N + M)	Binary edge betweenness centrality	0.3	Binary edge betweenness centrality	0.3	Edge neighborhood overlap	0.3	Edge neighborhood overlap	0.3	Binary edge betweenness centrality	0.4
FL(N)	Community structure	0.4	Matching index	0.1	Binary edge betweenness centrality	0.3	Binary edge betweenness centrality	0.3	Edge neighborhood overlap	0.1
FL(M)	R-peri calcarine <->L-pars opercularis	0.5	R-lateral orbitofrontal <->L-lateral orbitofrontal	1.0	R-medial orbitofrontal <->L-insula	0.8	R-pars opercularis <->L-lateral orbitofrontal	0.3	R-pars orbitalis <->L-lateral orbitofrontal	0.3
FL(N + M)	Binary edge betweenness centrality	0.3	Binary edge betweenness centrality	0.3	Matching index	0.1	R-Transverse temporal <->R-superior temporal	0.3	Community structure	0.4
FI(N)+FL(N)	FL(N): strengths	0.1	FI(N): binary edge betweenness centrality	0.4	FI(N): binary edge betweenness centrality	0.5	FI(N): Binary edge betweenness centrality	0.6	FI(N): binary edge betweenness centrality	0.7
FI(M) + FL(M)	FL(M): R-pars opercularis ->L-lateral orbitofrontal	0.3	FL(M): R-pars orbitalis <->L-lateral orbitofrontal	0.3	FL(M): R-pars triangularis <->L-lateral orbitofrontal	0.3	FL(M): R-peri calcarine <->L-lateral orbitofrontal	0.3	FL(M): R-postcentral <->L-lateral orbitofrontal	0.3
FI(N + M) + FL(N + M)	FL(N): strengths	0.1	FL(M): R-pars opercularis <->L-lateral orbitofrontal	0.3	FL(M): R-pars orbitalis <->L-lateral orbitofrontal	0.3	FL(M): R-pars triangularis <->L-lateral orbitofrontal	0.3	FL(M): R-peri calcarine <->L-lateral orbitofrontal	0.3

The features were computed using fiber connectivity (FI) and flow connectivity (FL) methods using a variety of graph-based network measures (N) and the raw connectivity matrices (M). The network measures were computed from binary and weighted connectivity matrices that were filtered using a proportional threshold ranking from 0.1 to 1.0 (meaning all edges are retained) at intervals of 0.1. The features are shown along with their corresponding threshold (Th.). The ranking is derived from the support vector machine classification boundary and is averaged over each of the 10 cross-validated folds and 30 repeat runs. In cases that use features including the raw connectivity matrices at different thresholds, the label includes the 2 regions from the FreeSurfer segmentation that an edge connects. The symbol "<->" represents the undirected edge connecting the 2 regions in the connectivity network.
Key: EMCI, early mild cognitive impairment; L, left; R, right.

2 classes of data, and the slack variables are added to create soft margins to separate most of the points.

Our classification design was to test the information provided by the connectivity features with repeated stratified 10-fold cross-validation as recommended by Kohavi (1995). For the results in the cross-validation, our performance metrics were accuracy, sensitivity, and specificity. We repeated the cross-validation 30 times, which allows us to use paired-sample t tests to statistically compare different feature subsets based on their classification performance.

For each classifier, we learned that the features were ranked by their relationship to the hyperplane (De Martino et al., 2008). The ranking was computed by sorting in decreasing order the $|w|$ values from the hyperplane. Features with high values mean they contribute the most to the final boundary between the classes. In our experiments, we averaged the feature ranking across all folds within repeated cross-validation instances. These rankings will tell what network measure or what element of a connectivity matrix was most important to the classifier in the context of all other features in a feature set of interest.

2.4. Experiments

We designed experiments to test the utility of different subsets of features to identify differences between sets of 2 disease states from our data. Our metrics were the accuracy, sensitivity, and specificity from stratified 10-fold cross-validation that was repeated 30 times comparing controls versus AD, controls versus EMCI, controls versus LMCI, and EMCI versus LMCI. In each of these classification problems, we used 9 different sets of features: the fiber connectivity matrix, (FI(M)), the flow connectivity matrix (FL(M)), the fiber network measures (FI(N)), the flow network measures (FL(M)), and the combinations of these sets as FI(N + M), FL(N + M), FI(N) + FL(N), FI(M) + FL(M), and FI(N + M) + FL(N + M). Each of these sets of features was organized into a matrix and then fed into the SVM algorithm using a repeated, stratified 10-fold cross-validation design. A summary of our experimental design is in Fig. 2.

3. Results

Figures 3–6 show bar charts of the results for each of our 4 classification problems using the 9 different subsets of features. These include controls versus AD (Fig. 3), controls versus EMCI (Fig. 4), controls versus LMCI (Fig. 5), and EMCI versus LMCI (Fig. 6). It shows the accuracy, sensitivity, and specificity as percentages for each of the 9 feature sets including FI(N), FI(M), FI(N + M), FL(N), FL(M), FL(N + M), FI(N) + FL(N), FI(M) + FI(M), and FI(N + M) + FL(N + M) along with their 95% confidence intervals over the stratified 10-fold cross-validated results that were repeated 30 times. For controls versus AD, we found feature set FI(N) + FL(N) had the highest accuracy of 78.2%, and using paired-sample t tests ($p > 0.05$), we found it was not statistically different in performance from FI(N) and FI(N + M). FI(N + M) had the highest accuracy of 59.2% for the controls versus EMCI classifier and was not

Table 5
The top 5 ranked features from each of the 9 feature subsets in the controls versus LMCI classification problem

Controls vs. LMCI										
Feature set	Rank 1/Th.		Rank 2/Th.		Rank 3/Th.		Rank 4/Th.		Rank 5/Th.	
FI(N)	Matching index	0.1	Matching index	0.2	Binary edge betweenness centrality	0.4	Binary edge betweenness centrality	0.4	Binary edge betweenness centrality	0.5
FI(M)	R-inferior parietal <->L-temporal pole	1.0	R-inferior temporal <->L-temporal pole	1.0	R-isthmus of the cingulate <->L-temporal pole	1.0	R-lateral occipital <->L-temporal pole	1.0	R-lateral orbitofrontal <->L-temporal pole	1.0
FI(N + M)	Binary edge betweenness centrality	0.4	Matching index	0.1	Binary edge betweenness centrality	0.4	Binary edge betweenness centrality	0.5	Binary edge betweenness centrality	0.6
FL(N)	Binary local efficiency	0.2	Matching index	0.1	Matching index	0.1	Edge neighborhood overlap	0.4	Edge neighborhood overlap	0.4
FL(M)	R-supramarginal <->L-medial orbitofrontal	1.0	L-pars opercularis <->L-lingual	0.9	L-supramarginal <->L-inferior parietal	0.9	L-frontal pole <->L-inferior parietal	0.9	L-temporal pole <->L-inferior parietal	0.9
FL(N + M)	Binary local efficiency	0.2	Matching index	0.1	Edge neighborhood overlap	0.4	Edge neighborhood overlap	0.4	Edge neighborhood overlap	0.5
FI(N) + FL(N)	FI(N): edge neighborhood overlap	0.5	FI(N): edge neighborhood overlap	0.6	FI(N): edge neighborhood overlap	0.7	FI(N): edge neighborhood overlap	0.8	FI(N): edge neighborhood overlap	0.5
FI(M) + FL(M)	FL(M): R-pars opercularis <->L-banks of the superior temporal sulcus	0.4	FL(M): R-pars orbitalis <->L-banks of the superior temporal sulcus	0.4	FL(M): L-supramarginal <->L-inferior parietal	0.9	FL(M): R-pars triangularis <->L-banks of the superior temporal sulcus	0.4	FL(M): L-frontal pole <->L-inferior parietal	0.9
FI(N + M) + FL(N + M)	FI(N): binary edge betweenness centrality	0.5	FI(N): binary edge betweenness centrality	0.6	FI(N): binary edge betweenness centrality	0.7	FI(N): binary edge betweenness centrality	0.8	FI(N): binary edge betweenness centrality	0.9

The features were computed using fiber connectivity (FI) and flow connectivity (FL) methods using a variety of graph-based network measures (N) and the raw connectivity matrices (M). The network measures were computed from binary and weighted connectivity matrices that were filtered using a proportional threshold ranking from 0.1 to 1.0 (meaning all edges are retained) at intervals of 0.1. The features are shown along with their corresponding threshold (Th.). The ranking is derived from the support vector machine classification boundary and is averaged over each of the 10 cross-validated folds and 30 repeat runs. In cases that use features including the raw connectivity matrices at different thresholds, the label includes the 2 regions from the FreeSurfer segmentation that an edge connects. The symbol "<->" represents the undirected edge connecting the 2 regions in the connectivity network.
Key: LMCI, late mild cognitive impairment; L, left; R, right.

significantly different in performance from FI(N + M) + FL(N + M). In the case of controls versus LMCI, FL(N) had the highest accuracy of 62.8% and was significantly better in performance than all other feature sets. EMCI versus LMCI performed best with FI(N) + FL(N) reaching an accuracy of 63.4% and was significantly different than all other feature sets.

In addition to the bar charts, we ranked the top 5 features for each classification problem and feature set in Tables 3–6. Each of the top features is also listed with its corresponding threshold value. A multidimensional feature such as "edge neighborhood overlap" may be listed multiple times at the same threshold for a single feature set and classification problem because the ranking is differentiating between parts of the feature vector for that single network measure. We also include the specific labels for elements in the connectivity matrices that were highly ranked, and the symbol "<->" represents the undirected edge between the 2 regions on the cortex.

4. Discussion

For classification of normal elderly controls relative to people with AD, Table 1 shows that FI(N) + FL(N) has the highest classification accuracy. Even so, when these features combined with additional features, the accuracy does go down in some instances. FI(N + M) was able to distinguish controls versus EMCI the best, and FL(N) was the best for distinguishing healthy controls versus LMCI. In the EMCI versus LMCI classification experiments, we again saw a combination of network measures FI(N) + FL(N) that produced the best results. The results show that when studying LMCI including flow-based network measures can have an advantage in distinguishing class differences and may be useful for studying other aspects of LMCI. In the case of EMCI and AD, the performance of classification could be optimal based on fiber measures alone, although the addition of flow in AD may have slightly higher accuracy.

In addition to offering a principled approach to select or rank the importance of connectivity features for this kind of classification problem, we provided a proof of concept and framework for using SVMs as a metric for use with brain connectivity data. We recently used it to choose the architecture of the connectivity matrix by selecting the best nodes or regions of the cortex. This adaptive cortical parcellation was created based on a framework to evaluate different cortical parcellations by their accuracy from diagnostic classifiers, such as SVMs (Prasad et al., 2014).

Learning algorithms, such as SVM, Adaboost, and random forest classification, can be sensitive to the feature set used. We note that other schemes may be used, and their effects could also be useful to categorize this dataset and other related data or even filter out features in each of the feature sets we studied. Other classification techniques that may be effective include a variation of manifold learning used by Iglesias et al. (2011b) to classify AD using registration- and overlap-based similarity measures. Alternatively, we could organize the features into a tensor representation for multilinear subspace learning (Tao et al., 2007).

These other algorithms may be particularly adept at classification of AD because of how well they can build a model with the relatively limited number of subjects in these studies, by contrast with the large number of features for each subject. New subjects are continually being added to the ADNI dataset, and more training data would give us a stronger and more secure

Table 6
The top 5 ranked features from each of the 9 feature subsets in the EMCI versus LMCI classification problem

EMCI vs. LMCI										
Feature set	Rank 1/Th.		Rank 2/Th.		Rank 3/Th.		Rank 4/Th.		Rank 5/Th.	
FI(N)	Edge neighborhood overlap	0.3	Edge neighborhood overlap	0.3	Matching index	0.1	Binary Edge betweenness centrality	0.4	Binary Edge betweenness centrality	0.4
FI(M)	L-frontal pole <->L-supramarginal	0.8	L-temporal pole <->L-supramarginal	0.8	L-pars orbitalis <->L-lateral occipital	0.3	L-transverse temporal <->L-supramarginal	0.8	L-insula <->L-supramarginal	0.8
FI(N + M)	Edge neighborhood overlap	0.3	Edge neighborhood overlap	0.3	Matching index	0.1	R-transverse temporal <->R-lingual	0.8	Edge neighborhood overlap	0.4
FL(N)	Matching index	0.1	Community structure	0.3	Matching index	0.1	Binary Nodal betweenness centrality	0.1	Community structure	0.3
FL(M)	R-parahippocampal <->R-lingual	0.9	R-cuneus <->L-frontal pole	0.1	R-paracentral <->R-inferior parietal	0.1	R-inferior parietal <->R-entorhinal	0.3	R-isthmus of the cingulate <->L-superior temporal	0.6
FL(N + M)	Community structure	0.3	Matching index	0.1	Matching index	0.1	Community structure	0.3	Binary Nodal betweenness centrality	0.1
FI(N) + FL(N)	FL(N): community structure	0.3	FL(N): community structure	0.3	FL(N): community structure	0.3	FL(N): community structure	0.3	FL(N): binary community structure	0.3
FI(M) + FL(M)	FL(M): R-superior frontal <->L-peri calcarine	0.1	FL(M): R-superior parietal <->L-peri calcarine	0.1	FL(M): R-superior temporal <->L-peri calcarine	0.1	FL(M): R-supramarginal <->L-peri calcarine	0.1	FL(M): R-frontal pole <->L-peri calcarine	0.1
FI(N + M) + FL(N + M)	FL(N): community structure	0.3	FL(N): community structure	0.3	FL(N): community structure	0.3	FL(N): community structure	0.3	FL(N): community structure	0.3

The features were computed using fiber connectivity (FI) and flow connectivity (FL) methods using a variety of graph-based network measures (N) and the raw connectivity matrices (M). The network measures were computed from binary and weighted connectivity matrices that were filtered using a proportional threshold ranking from 0.1 to 1.0 (meaning all edges are retained) at intervals of 0.1. The features are shown along with their corresponding threshold (Th.). The ranking is derived from the support vector machine classification boundary and is averaged over each of the 10 cross-validated folds and 30 repeat runs. In cases that use features including the raw connectivity matrices at different thresholds, the label includes the 2 regions from the FreeSurfer segmentation that an edge connects. The symbol "<->" represents the undirected edge connecting the two regions in the connectivity network.
Key: EMCI, early mild cognitive impairment; LMCI, late MCI; L, left; R, right.

understanding of these relationships. With larger datasets, we can explore the absolute and relative performance of different features and biomarkers using deep learning (Hinton et al., 2006) or artificial neural networks that allow for a great deal of freedom and a richer model when there are multiple layers included (Bengio, 2009) and massive amounts of data available. Here, we chose SVM as it works well with relatively small samples and a larger number of features without having to apply regularization (Hastie et al., 2001).

The feature ranking approach we used leveraged the hyperplane from the SVM and gives a ranking of a feature in the context of all other features in the set we are studying. Other approaches such as univariate ranking by using *t* tests on a single feature (Chu et al., 2012) or by using regression on each feature (Polyn et al., 2005) give the importance of a single measure by itself but may miss cases when a feature by itself is weak, but in the context of other features, the feature set becomes highly discriminatory. There are also a variety of multivariate feature selection approaches being proposed in the literature. One method by Liu et al. (2013) addresses the geometric relationship of the target classes in AD structural MRI training data by using graph matching. Another approach combines univariate feature selection and multivariate recursive feature selection by using correlation-based ranking of single features. It then uses recursive and forward sequential feature selection to select a set of features that will include mostly the top-ranked features (Fan et al., 2007). In Cuingnet et al. (2011), the authors study 10 algorithms that classify AD using T1-weighted MRI and conclude that different feature selection methods did not greatly affect performance. In our case, we used the feature selection to evaluate a classifier and its features without removing or selecting features based on training data.

Different sets of features may uncover detail in the connectivity structure of the brain that is better for representing important changes in networks across the various phases or stages of AD. We can extend the framework in the present study to use different features such as those from dynamic simulations of connectivity (Prasad et al., 2013a) or connectivity measures that summarize the fibers from tractography using maximum density paths (Prasad et al., 2011a) that are registered (Prasad et al., 2011b) into the same space. We can then use the subset of features that best predict or classify a category in our data that could include effects of aging, severity of the disorder, or even those that emphasize parts of the network that are associated with the effects of risk genes for AD.

Disclosure statement

The authors have no potential, financial, or personal conflicts of interest, including relationships with other people or organizations, within 3 years of beginning the work submitted, that could inappropriately influence their work.

Acknowledgements

Algorithm development and image analysis for this study were funded, in part, by grants to PT from the National Institute of Biomedical Imaging and Bioengineering (NIBIB) (R01 EB008281, R01 EB008432, R21 EB01651) and by the National Institute on Aging (NIA) (P50 AG016570-019002, R01 AG040060, U01 AG024904-01), NIBIB, the National Institute of Mental Health, the US National Library of Medicine (R01 LM05639), and the National Center for Research Resources (AG016570, AG040060, EB01651, MH097268, LM05639, and RR019771 to PT). Data collection and sharing for this

project were funded by Alzheimer's Disease Neuroimaging Initiative (ADNI) (National Institutes of Health [NIH] grant U01 AG024904). ADNI is funded by the NIA, the NIBIB, and through contributions from the following: Abbott, Alzheimer's Association, Alzheimer's Drug Discovery Foundation, Amorfix Life Sciences Ltd, AstraZeneca, Bayer HealthCare, BioClinica Inc, Biogen Idec Inc, Bristol-Myers Squibb Company, Eisai Inc, Elan Pharmaceuticals Inc, Eli Lilly and Company, F. Hoffmann-La Roche Ltd, and its affiliated companies Genentech Inc, GE Healthcare, Innogenetics, N.V., IXICO Ltd, Janssen Alzheimer Immunotherapy Research & Development, LLC, Johnson & Johnson Pharmaceutical Research & Development LLC, Medpace Inc, Merck & Co Inc, Meso Scale Diagnostics LLC, Novartis Pharmaceuticals Corporation, Pfizer Inc, Servier, Synarc Inc, and Takeda Pharmaceutical Company. The Canadian Institutes of Health Research is providing funds to support ADNI clinical sites in Canada. Private sector contributions are facilitated by the Foundation for the NIH. The grantee organization is the Northern California Institute for Research and Education, and the study is coordinated by the Alzheimer's Disease Cooperative Study at the University of California, San Diego. ADNI data are disseminated by the Laboratory for Neuro Imaging at the University of Southern California. This research was also supported by NIH grants P30 AG010129 and K01 AG030514 from the National Institute of General Medical Sciences.

References

Aganj, I., Lenglet, C., Jahanshad, N., Yacoub, E., Harel, N., Thompson, P.M., Sapiro, G., 2011. A Hough transform global probabilistic approach to multiple-subject diffusion MRI tractography. Med. Image Anal. 15, 414–425.

Aganj, I., Lenglet, C., Sapiro, G., Yacoub, E., Ugurbil, K., Harel, N., 2010. Reconstruction of the orientation distribution function in single-and multiple-shell Q-ball imaging within constant solid angle. Magn. Reson. Med. 64, 554–566.

Basser, P., Pierpaoli, C., 1996. Microstructural and physiological features of tissues elucidated by quantitative diffusion-tensor MRI. J. Magn. Reson. B 111, 209–219.

Bengio, Y., 2009. Learning Deep Architectures for AI. Foundations and Trends in Machine Learning, vol. 2. Now Publishers Inc., Hanover, MA, pp. 1–127.

Chu, C., Hsu, A.L., Chou, K.H., Bandettini, P., Lin, C., 2012. Does feature selection improve classification accuracy? Impact of sample size and feature selection on classification using anatomical magnetic resonance images. Neuroimage 60, 59–70.

Cortes, C., Vapnik, V., 1995. Support-vector networks. Machine Learn. 20, 273–297.

Cui, Y., Wen, W., Lipnicki, D.M., Beg, M.F., Jin, J.S., Luo, S., Zhu, W., Kochan, N.A., Reppermund, S., Zhuang, L., Raamana, P.R., Liu, T., Trollor, J.N., Wang, L., Brodaty, H., Sachdev, P.S., 2012. Automated detection of amnestic mild cognitive impairment in community-dwelling elderly adults: a combined spatial atrophy and white matter alteration approach. Neuroimage 59, 1209–1217.

Cuingnet, R., Gerardin, E., Tessieras, J., Auzias, G., Lehéricy, S., Habert, M.O., Chupin, M., Benali, H., Colliot, O., Alzheimer's Disease Neuroimaging Initiative, 2011. Automatic classification of patients with Alzheimer's disease from structural MRI: a comparison of ten methods using the ADNI database. Neuroimage 56, 766–781.

De Martino, F., Valente, G., Staeren, N., Ashburner, J., Goebel, R., Formisano, E., 2008. Combining multivariate voxel selection and support vector machines for mapping and classification of fMRI spatial patterns. Neuroimage 43, 44–58.

Eskildsen, S., Coupé , P., Garćia-Lorenzo, D., Fonov, V., Pruessner, J., Collins, L., et al., 2012. Improving prediction of Alzheimer's disease using patterns of cortical thinning and homogenizing images according to disease stage. Medical Image Computing and Computer-Assisted Intervention—Miccai 2012: Novel Biomarkers for Alzheimer's Disease and Related Disorders Workshop, 79–90.

Fan, Y., Shen, D., Gur, R.C., Gur, R.E., Davatzikos, C., 2007. COMPARE: classification of morphological patterns using adaptive regional elements. IEEE Trans. Med. Imaging 26, 93–105.

Fischl, B., van der Kouwe, A., Destrieux, C., Halgren, E., Ségonne, F., Salat, D.H., Busa, E., Seidman, L.J., Goldstein, J., Kennedy, D., Caviness, V., Makris, N., Rosen, B., Dale, A.M., 2004. Automatically parcellating the human cerebral cortex. Cereb. Cortex 14, 11–22.

Fritzsche, K.H., Laun, F.B., Meinzer, H.P., Stieltjes, B., 2010. Opportunities and pitfalls in the quantification of fiber integrity: what can we gain from Q-ball imaging? Neuroimage 51, 242–251.

Gong, G., He, Y., Concha, L., Lebel, C., Gross, D.W., Evans, A.C., Beaulieu, C., 2009. Mapping anatomical connectivity patterns of human cerebral cortex using in vivo diffusion tensor imaging tractography. Cereb. Cortex 19, 524–536.

Guyon, I., Elisseeff, A., 2003. An introduction to variable and feature selection. J. Mach. Learn. Res. 3, 1157–1182.

Hagmann, P., Cammoun, L., Gigandet, X., Meuli, R., Honey, C.J., Wedeen, V.J., Sporns, O., 2008. Mapping the structural core of human cerebral cortex. PLoS Biol. 6, 1479–1493.

Hastie, T., Tibshirani, R., Friedman, J., 2001. The Elements of Statistical Learning. Springer, New York.

Hinton, G.E., Osindero, S., Teh, Y.W., 2006. A fast learning algorithm for deep belief nets. Neural Comput. 18, 1527–1554.

Holmes, C., Hoge, R., Collins, L., Woods, R., Toga, A., Evans, A., 1998. Enhancement of MR images using registration for signal averaging. J. Comput. Assist. Tomogr. 22, 324–333.

Iglesias, J.E., Jiang, J., Liu, C.Y., Tu, Z., 2011b. Classification of Alzheimer's disease using a self-smoothing operator. Med. Image Comput. Comput. Assist. Interv. 14, 58–65.

Iglesias, J., Liu, C., Thompson, P., Tu, Z., 2011a. Robust brain extraction across datasets and comparison with publicly available methods. IEEE Trans. Med. Imaging 30, 1617–1634.

Ingalhalikar, M., Smith, A., Parker, D., Satterthwaite, T.D., Elliott, M.A., Ruparel, K., Hakonarson, H., Gur, R.E., Gur, R.C., Verma, R., 2013. Sex differences in the structural connectome of the human brain. Proc. Natl. Acad. Sci. U. S. A. 111, 823–828.

Jahanshad, N., Aganj, I., Lenglet, C., Joshi, A., Jin, Y., Barysheva, M., McMahon, K.L., de Zubicaray, G.I., Martin, N.G., Wright, M.J., Toga, A.W., Sapiro, G., Thompson P.M., 2011. Sex differences in the human connectome: 4-Tesla high angular resolution diffusion imaging (HARDI) tractography in 234 young adult twins. 2011 IEEE International Symposium on Biomedical Imaging: From Nano to Macro, 939–943.

Jenkinson, M., Bannister, P., Brady, M., Smith, S., 2002. Improved optimization for the robust and accurate linear registration and motion correction of brain images. Neuroimage 17, 825–841.

Klöppel, S., Stonnington, C., Chu, C., Draganski, B., Scahill, R., Rohrer, J., Fox, N., Jack, C., Ashburner, J., Frackowiak, R., 2008. Automatic classification of MR scans in Alzheimer's disease. Brain 131, 681–689.

Kohannim, O., Hua, X., Hibar, D., Lee, S., Chou, Y., Toga, A., Jack, C., Weiner, M., Thompson, P., 2010. Boosting power for clinical trials using classifiers based on multiple biomarkers. Neurobiol. Aging 31, 1429–1442.

Kohavi, R., 1995. A study of cross-validation and bootstrap for accuracy estimation and model selection. International Joint Conference on Artificial Intelligence, Vol. 14, pp. 1137–1145.

Leow, A., Yanovsky, I., Chiang, M., Lee, A., Klunder, A., Lu, A., Becker, J., Davis, S., Toga, A., Thompson, P., 2007. Statistical properties of Jacobian maps and the realization of unbiased large-deformation nonlinear image registration. IEEE Trans. Med. Imaging 26, 822–832.

Liu, F., Suk, H.I., Wee, C.Y., Chen, H., Shen, D., 2013. High-order graph matching based feature selection for Alzheimer's disease identification. Med. Image Comput. Comput. Assist. Interv. 16 (Pt 2), 311–318.

Mueller, S., Weiner, M., Thal, L., Petersen, R., Jack, C., Jagust, W., Trojanowski, J., Toga, A., Beckett, L., 2005. Ways toward an early diagnosis in Alzheimer's disease: the Alzheimer's Disease Neuroimaging Initiative (ADNI). Alzheimers Dement. 1, 55–66.

Nir, T., Jahanshad, N., Toga, A., Jack, C., Weiner, M., Thompson, P., 2012. Connectivity network breakdown predicts imminent volumetric atrophy in early mild cognitive impairment. Medical Image Computing and Computer-Assisted Intervention—MICCAI 2012: Multimodal Brain Image Analysis Workshop, vol. 15, 41–50.

Peng, H., Long, F., Ding, C., 2005. Feature selection based on mutual information criteria of max-dependency, max-relevance, and min-redundancy. IEEE Trans. Pattern Anal. Mach. Intell. 27, 1226–1238.

Polyn, S.M., Natu, V.S., Cohen, J.D., Norman, K.A., 2005. Category-specific cortical activity precedes retrieval during memory search. Science 310, 1963–1966.

Prasad, G., Burkart, J., Joshi, S.H., Nir, T.M., Toga, A.W., Thompson, P.M., 2013a. A dynamical clustering model of brain connectivity inspired by the N-body problem. Medical Image Computing and Computer-Assisted Intervention—MICCAI 2013: Multimodal Brain Image Analysis Workshop, vol. 16, 129–137.

Prasad, G., Jahanshad, N., Aganj, I., Lenglet, C., Sapiro, G., Toga, A., Thompson, P., 2011a. Atlas-based fiber clustering for multi-subject analysis of high angular resolution diffusion imaging tractography. 2011 IEEE International Symposium on Biomedical Imaging: From Nano to Macro, 276–280.

Prasad, G., Joshi, S., Jahanshad, N., Villalon, J., Aganj, I., Lenglet, C., Sapiro, G., McMohan, K., de Zubicaray, G., Martin, N., Wright, M., Toga, A., Thompson, P., 2011b. White matter tract analysis in 454 adults using maximum density paths. Medical Image Computing and Computer-Assisted Intervention—MICCAI 2011: Computational Diffusion MRI Workshop, 1–12.

Prasad, G., Joshi, S., Nir, T., Toga, A., Thompson, P., 2013b. Flow-based network measures of brain connectivity in Alzheimer's disease. 2013 IEEE International Symposium on Biomedical Imaging: From Nano to Macro, 258–261.

Prasad, G., Joshi, S., Thompson, P., 2014. Optimizing brain connectivity networks for disease classification using EPIC. 2014 IEEE International Symposium on Biomedical Imaging: From Nano to Macro.

Prasad, G., Nir, T., Toga, A., Thompson, P., 2013c. Tractography density and network measures in Alzheimer's disease. 2013 IEEE International Symposium on Biomedical Imaging: From Nano to Macro, 692–695.

Rubinov, M., Sporns, O., 2010. Complex network measures of brain connectivity: uses and interpretations. Neuroimage 52, 1059–1069.

Sled, J., Zijdenbos, A., Evans, A., 1998. A nonparametric method for automatic correction of intensity nonuniformity in MRI data. IEEE Trans. Med. Imaging 17, 87–97.
Smith, S., 2002. Fast robust automated brain extraction. Hum. Brain Mapp. 17, 143–155.
Tao, D., Li, X., Wu, X., Hu, W., Maybank, S.J., 2007. Supervised tensor learning. Knowledge Inf. Syst. 13, 1–42.
Tibshirani, R., 1996. Regression shrinkage and selection via the lasso. J. R. Stat. Soc. Ser. B (Methodological) 58, 267–288.
Tuch, D., 2004. Q-ball imaging. Magn. Reson. Med. 52, 1358–1372.
Zhang, D., Shen, D., 2011. Semi-supervised multimodal classification of Alzheimer's disease. 2011 IEEE International Symposium on Biomedical Imaging: From Nano to Macro, 1628–1631.